Nanoscale

Accepted Manuscript

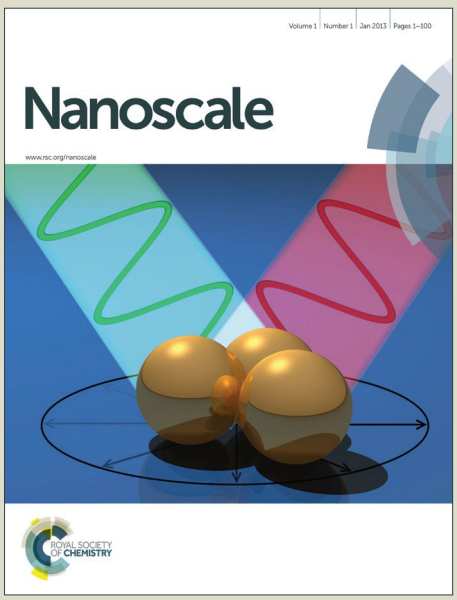

ROYAL SOCIETY OF CHEMISTRY

www.rsc.org/nanoscale

ARTICLE TYPE www. rsc.org/xxxxxx | XXXXXXXX

STEM-EELS Analysis of Multipole Surface Plasmon Modes in Symmetry-Broken AuAg Nanowire Dimers

Ina Schubert,*[a] Wilfried Sigle,[b] Peter A. van Aken,[b] Christina Trautmann,[a,c] and Maria Eugenia Toimil-Molares[a]

Received Xth XXXXXXXXXX 20XX, Accepted Xth XXXXXXXXX 20XX
First published on the web Xth XXXXXXXXXX 200X
DOI: 10.1039/b000000x

Surface plasmon coupling in nanowires separated by small gaps generates high field enhancements at the position of the gap and is thus of great interest for sensing applications. It is known that the nanowire dimensions and in particular the symmetry of the structures has strong influence on the plasmonic properties of the dimer structure. Here, we report on multipole surface plasmon coupling in symmetry-broken AuAg nanowire dimers. Our dimers, consisting of two nanowires with different lengths and separated by gaps of only 10 to 30 nm, were synthesized by pulsed electrochemical deposition in ion track-etched polymer templates. Electron energy-loss spectroscopy in scanning transmission electron microscopy allows us to resolve up to nine multipole order surface plasmon modes of these dimers spectrally separated from each other. The spectra evidence plasmon coupling between resonances of different multipole order, resulting in the generation of additional plasmonic modes. Since such complex structures require elaborated synthesis techniques, dimer structures with complex composition, morphology and shape are created. We demonstrate that finite element simulations on pure Au dimers can predict the generated resonances in the fabricated structures. The excellent agreement of our experiment on AuAg dimers with finite integration simulations using CST microwave studio manifests great potential to design complex structures for sensing applications.

Keywords: symmetry-broken nanowire dimers, electron energy-loss spectroscopy, scanning transmission electron microscopy, multipole surface plasmon, antibonding mode, nanogap

1 Introduction

Symmetry-broken nanostructures are currently attracting great attention in the field of plasmonics.[1–7] In nanostructures, two groups of surface plasmonic modes can be distinguished by their different net dipole moment. Modes that possess a high net dipole moment are named bright modes, while modes with a zero or very small net dipole moment are defined as dark modes.[1] Using an incident plane wave as excitation source, in symmetrical structures only the bright modes are optically active. In contrast, the asymmetry in symmetry-broken structures can result in a small net dipole moment of a dark mode. Consequently, in these structures dark modes can be excited with a plane wave which makes these nanostructures very interesting for sensing applications: The optical excitation of the dark modes in asymmetrical structures can enhance the flexibility to sense various analytes. In addition, the sensitivity of surface enhanced Raman spectroscopy (SERS) and fluorescence spectroscopy can be enhanced by tuning a bright mode to the excitation wavelength and a dark mode to the emission wavelength of the experiment, respectively.[8,9] Furthermore, in asymmetrical structures, the interference of a bright and a dark resonance that overlap in their energy can result in the generation of a Fano resonance with asymmetrical lineshape.[2–7] A Fano resonance is extremely sensitive to changes of the dielectric background, enabling the detection of very small analyte concentrations.[10,11]

A symmetry-break can be obtained by designing complex structures consisting of particles of various materials[12–14], different sizes and shapes[13,15–17] or oriented under different angles to each other.[16,18,19] Moreover, it can also be generated by randomly created defects and surface roughness resulting from the synthesis process.[20,21] To achieve a better understanding of the resonances in symmetry-broken systems, investigations with systematic parameter control are crucial.

In particular, nanowire dimers, consisting of two nanowires separated by a small gap, are ideal model systems for the detailed analysis of surface plasmon modes since they exhibit several multipole order modes in their spectra[22] and since high field enhancements can be excited at the gap position.[23] Fur-

[a] *GSI Helmholtzzentrum für Schwerionenforschung GmbH, Planckstr. 1, Darmstadt, Germany Fax: 49 6159 713266 ; Tel: 49 6159 712033; E-mail: i.schubert@gsi.de*
[b] *Max Planck Institute for Intelligent Systems, Heisenbergstr. 3, Stuttgart, Germany*
[c] *Technische Universität Darmstadt, Darmstadt, Germany*

thermore, a synthesis method exists that allows precise control of the nanowire dimensions.[24] For symmetrical dimers, it has been demonstrated experimentally using electron energy-loss spectroscopy[25,26] and theoretically[27] that surface plasmon coupling results in splitting into bonding - antibonding mode pairs and that the energy difference between bonding and antibonding mode decreases with increasing multipole order. For the dimer systems, the bonding mode is a bright mode, while the antibonding mode is dark. By tuning the dimensions of the two wires, surface plasmon coupling can be investigated in detail. For symmetry-broken nanorod dimers of short length (<200 nm), several authors have demonstrated that a symmetry-break allows optical detection of the antibonding dipole mode of the system.[15,16,18] The energy difference between first-order bonding and antibonding modes and the excitation efficiency of these modes depend sensitively on the ratio of their length, gap size and angle between the two rods. Based on calculations, it has been predicted that in symmetry-broken dimers consisting of two different materials such as Pd and Ag Fano resonances can be created[14]. While several authors have investigated so far surface plasmon coupling in symmetry-broken structures for the dipolar modes, analysis of the higher multipolar order modes is rare. Using extinction spectroscopy, it has been shown recently that for given rod dimensions not only same order modes but also different order modes can couple.[28]

Here, we report on the plasmonic properties of symmetry-broken AuAg nanowire dimers. We demonstrate for the first time surface plasmon coupling of high multipole order modes in asymmetrcial nanowire dimers and compare the resulting spectra to finite element simulations on Au dimers.

Dimers with diameter of $\sim$ 100 nm and different lengths varying between 500 nm and 1.5 μm were fabricated by pulsed electrodeposition of Au and Ag in ion-track etched polymer membranes. We have performed electron energy-loss spectroscopy measurements in scanning transmission electron microscopy (STEM-EELS) and energy filtered transmission electron microscopy (EFTEM) on these structures. The measurements allowed us to identify all the surface plasmonic modes in a very broad energy range and at the same time obtain high-resolution images that depict the nanowire dimer parameters. The fabrication of elaborated systems, such as nanowire dimers, requires complicated synthesis techniques that result in complex nanostructure parameters, such as composition, surface morphology, crystallinity and gap shape. For these systems, the dispersion relations are up to now not known. We have therefore compared the experimental results to finite integration simulations obtained with CST Microwave Studio on pure Au dimers.[29] The present comparison allows us to investigate whether simple finite element simulations with a commercially available program on pure Au wires can predict all the excited modes in the complex synthesized dimers, which is very important for applications of these structures. Compared to the previously published results on symmetry-broken dimers,[28] we furthermore analysed experimentally the surface plasmon modes with the very high spatial resolution of few nanometres of STEM-EELS and identified the excited modes dependent on the position of the exciting electron beam. The dimers allowed us to experimentally verify mode coupling between multipole modes of differing multiple order. This will enable us to apply the dimers as sensing devices in different wavelength regimes by modifying only its asymmetry. Our results evidence a strategy for tuning surface plasmons of symmetry-broken nanowire dimers to specific resonance energies.

2 Results and Discussion

We synthesized asymmetrical AuAg dimers by electrochemical deposition in ion-track etched polymer templates as described in the Experimental section. We analysed the plasmonic properties of a dimer with $L_1 = 1036 \pm 10$ nm, $L_2 = 656 \pm 10$ nm, $D = 76 \pm 10$ nm and gap size of ~ 12 nm by STEM-EELS. Due to our synthesis technique, the experimental prepared dimer consisted of a core of Au:Ag atoms in the ratio 60:40 with a few nanometre thin Au shell.[30] We start the discussion with the simulation of a pure Au nanowire dimer with the finite element programme CST microwave studio. Afterwards, we present the experimentally obtained results on the AuAg dimer and study whether the experimental results of such complex structures can be predicted by the finite element simulations of pure Au dimers.

The finite element simulation for this Au dimer (red line) as well as for two single nanowires with length $L_1 = 1036$ nm (green) and $L_2 = 656$ nm (blue) are shown in Figure 1. Figure 1a shows schematically a nanowire dimer and defines its parameters L_1, L_2 as the length of the long and the short nanowire, respectively and D as its diameter. In the simulation, the surface plasmons are excited via a small dipole located 1 nm from the nanowire surface (black crosses) and the spectra were calculated at the opposite end (black dots). In Figure 1b the spectra calculated for the three structures are depicted. The corresponding schematics of the structures are shown on the right. The vertical lines denote the resonance maxima of the modes for the two structures. For the short nanowire (blue spectrum), the three peaks are assigned to the first three multipole modes with two, three, and four electric field maxima along the wire. Their energies are $E_{l=1} = 0.65 \pm 0.01$ eV, $E_{l=2} = 1.30 \pm 0.01$ eV and $E_{l=3} = 1.82 \pm 0.01$ eV. For the long nanowire (green spectrum) the first four modes with energies $E_{l=1} = 0.44 \pm 0.01$ eV, $E_{l=2} = 0.87 \pm 0.01$ eV, $E_{l=3} = 1.29 \pm 0.01$ eV and $E_{l=4} = 1.64 \pm 0.01$ eV are visible. For both wires, the surface charge distributions corresponding to these modes are schematically shown on top of each

of the peaks. As expected, all surface plasmon modes of the long wire are shifted to lower energies compared to the modes of the equal multipole order of the short wire. Note that for these nanowire dimensions, the peak of the $l = 3$-mode of the long wire and the $l = 2$-mode of the short wire are excited at the same energy. The spectrum of the dimer (red) reveals that all dimer modes are excited at energies close to the modes of either the short or the long single wire, namely $E_1 = 0.41 \pm 0.01$ eV, $E_2 = 0.62 \pm 0.01$ eV, $E_3 = 0.86 \pm 0.01$ eV, $E_4 = 1.21 \pm 0.01$ eV, $E_5 = 1.36 \pm 0.01$ eV, $E_6 = 1.64 \pm 0.01$ eV and $E_7 = 1.82 \pm 0.01$ eV. The corresponding electric field distributions (E_z-component) for these seven modes are presented on top. Shown is the xy-plane shifted by 25 nm in z-direction to a lateral cut through the nanowire. The amplitude of the electric field reveals that the first ($E_1 = 0.41$ eV) and the third mode ($E_3 = 0.86$ eV) have two respectively three very intense maxima along the long wire. These modes are very close in energy to the first and second mode of the long wire, the resonance condition is fullfilled for this wire, and an intense standing wave pattern is revealed. For the short wire, the resonance condition is not fulfill, leading to a lower amplitude and a more asymmetric field distribution. At the energy of the second mode ($E_2 = 0.62$ eV), the amplitude is slightly higher along the short wire. In this case the resonance condition is only fullfilled for the short wire. The redshift of these three dimer resonances compared to the corresponding single-wire resonances are attributed to the plasmon coupling between the wires via the gap.

The field distributions corresponding to the modes labelled four and five, reveal almost equally intense maxima along the two nanowires. In both cases, four maxima are excited along the long wire and three along the short one. Studying the direction of the electric field, we find that the lower energy mode (E = 1.21 eV) has the form of a bonding mode, e.g. negative and positive field maxima at opposite sides of the gap. In contrast, the higher energy mode (E = 1.36 eV) is an antibonding mode with maxima of the same sign located at each sides of the gap. Please note that in the figure the E_z-component is depicted with causes that the bonding mode reveals a nodal line at the gap position and the antibonding mode not. The opposite would be expected if the y-component would be shown. The generation of these two dimer modes predicts thus the surface plasmon hybridisation of the third-order mode of the long wire and the second-order mode of the short wire, excited at the same energy, which couple and form a bonding-antibonding mode pair. Finally, for the sixth mode at 1.64 eV the resonance condition is fullfilled for the long wire and at 1.82 eV only for the short wire.

In the following part the measurements are presented. Experimentally, it is well established that EFTEM and STEM-EELS are excellent methods to study surface plasmon modes with high spatial resolution.[17,25,26,31–34] The energy-loss probability of the electrons depends on the electric field component in the direction of the electron beam (defined as z-direction).[35–37] Positions of a high energy-loss probability along a nanowire can thus be attributed to positions of electric field maxima generated by surface plasmons. The energy corresponding to a peak in the low-loss region of the EEL spectrum defines the energy necessary to excite the corresponding surface plasmon mode.

Figure 2a shows an EFTEM series measured on the AuAg nanowire dimer of same dimensions L_1, L_2 and D described above. In EFTEM a monochromated parallel electron beam is used to illuminate the complete nanowire dimer. An energy-selecting slit at the dispersive plane allows only electrons with a chosen energy-loss to pass and form the two-dimensional image.[38] The energy selecting slit of the monochromator and the energy filter used for this experiment had both a width of 0.2 eV. Each image of the series originates only from electrons that have experienced an energy-loss in an interval of 0.2 eV between 0.5-1.7 eV. The color indicates the energy-loss probability.

Figure 2b depicts a color map consisting of 102 STEM-EEL spectra that are obtained by scanning a focused electron beam along the red arrow. The average distance of the scan line to the nanowire surface is ~ 15 nm. It is not performed up to the nanowire end due to the slight bending of the wire leading to a larger distance between electron beam and wire and thus to low counting statistics. In the map, regions of high energy-loss probability are visible by yellow and white color. Regions of blue color indicate low energy-loss probability. In Figure 2c three single spectra are shown that are measured at the positions of the three colored dots in the TEM image. The dots adopt the color of the corresponding spectra.

The STEM-EEL spectra allow us to collect data of the surface plasmon modes with high energetic resolution. With the EFTEM method at very short acquisition times a much larger two-dimensional area than possible with STEM-EELS can be investigated. The EFTEM images thus help to visualize the different modes.

We have marked the energies of the different modes in the map and the spectra by green, blue or light blue vertical arrows and enumerate these modes from one to nine. At higher energies, the resonances cannot be clearly resolved. Each image of the EFTEM series in Figure 2a can be attributed to one of these modes from two to seven. For the first mode no EFTEM image could be measured since this mode is very close in energy to the zero-loss peak.

The green spectrum reveals peaks at 0.33 ± 0.02 eV, 0.72 ± 0.02 eV, 0.98 ± 0.02 eV, 1.13 ± 0.02 eV 1.37 ± 0.02 eV, 1.65 ± 0.02 eV while in the blue spectrum most intense peaks at the energies of 0.51 ± 0.02 eV, 0.98 ± 0.02 eV, 1.13 ± 0.02 eV, 1.52 ± 0.02 eV and 1.86 ± 0.02 eV are resolvable. We find that the spectrum measured at the gap position (red) displays

peaks at the same energies as the spectrum at the end of the long (green) and also the short (blue) wire. An exception to this is the mode at 0.98 eV where we find a peak in the green as well as in the blue spectrum but not in the red one. For energies higher than 1.3 eV the quality of this spectrum in not sufficient to resolve peaks.

We compare in the following the peaks in our STEM-EELS map and the EFTEM images to the modes that we identified in our simulation. In the experiment, the modes labelled 1,3,6,8 reveal more intense maxima along the long, and and the modes 2,7,9 along the short wire. Field enhancements are also observed along the second wire, however they are much weaker than for the other one. An example are the two shoulders at low and high energy of the peak at 0.51 eV. These modes (1-3 and 6-9) can, in good agreement with our simulation, be assigned to the modes that are only resonant for one of the wires.

Furthermore, our data experimentally reveals that surface plasmon coupling between the second order mode of the short wire and the third order mode of the longer wire occurs, resulting in the bonding-antibonding mode pairs, visible in modes 4 and 5. Both, EFTEM images and STEM-EELS map show that for the modes 4 and 5 the maxima along the two wires have same intensity. The high-resolution STEM-EELS map depicts no peak at the position of the gap for the bonding mode. This has already been reported for symmetrical dimers and can be understood from symmetry arguments [17,25,32] because placing the electron beam at the position of the gap can only lead to a symmetrical charge distribution at both gap edges. In addition, the intensity maxima of the bonding modes are slightly shifted in the direction of the gap, while for the antibonding modes the maxima are shifted in the opposite direction. This is again in agreement with the symmetrical dimers and is ascribed to the repulsion between the charges of opposite or equal sign on opposite sites of the gap, respectively. The peaks at the end of the short wire are difficult to distinguish in the map due to the rounding of the nanowire ends which leads to a larger distance between the scan line and the nanowire tips. To enhance their visibility, we have marked for these two modes the positions of the maxima by red circles as identified when varying the color scaling.

Each of the modes identified in the experiment can be assigned to one of the modes depicted in the simulation of the pure Au dimer. This demonstrates that our simulation is a good model system to predict the excited spectrum of our fabricated structures. We observe however that certain differences between simulation and experiment exist: The experimental obtained resonance energies are shifted to lower energies compared to the simulated resonance energies. The deviation in energy is attributed to the Ag content in our synthesized wires (see Experimental) as well as to the Si_3N_4 substrate, which was not considered in our simulation. However, also the comparison for much less complex systems, such as a single pure Au nanowire, revealed a resonance shift between simulation and experiment.[34] Moreover, our simulation does not allow to predict the specific positions of the surface plasmon maxima. This can be understood from the different positions of the excitation source in simulation and experiment, but it is also assigned to the complex shape and surface morphology. An obvious example is the mode labelled with number seven. For this mode, the STEM-EELS map and the simulation reveal two intense maxima along the short wire. In the simulation, these two maxima reveal the same intensity. In the experiment, the intensity of the maxima closer to the gap is higher than for the other one. To obtain these informations the detailed STEM-EELS measurements are unavoidable.

We additionally verified if the mode coupling in our synthesized wires can also be predicted easily by the effective wavelength scaling formula given by Novotny.[39] The effective wavelength scaling formula states that the energies of the different multipole modes of two wires coincide if the relation $\frac{L_1}{L_2} = \frac{l_1}{l_2}$ is valid, l_1 and l_2 being the respective multipole orders of the mode of the long and short wire. Mode hybridisation is expected if two modes coincide in their energy. For the second- and third-order mode of two wires, we thus expect coupling for $\frac{L_1}{L_2} \approx 1.5$. This value is in good agreement with the ratio of the here investigated dimer which is $\beta = \frac{L_1}{L_2} = 1.58 \pm 0.03$. To further verify this scaling law, we have additionally investigated the coupling properties for two other asymmetric dimers that have higher and lower β values, respectively.

In Figure 3a the dimer is formed by two wires with diameter $D = 100 \pm 10$ nm, and lengths $L_1 = 935 \pm 10$ nm and $L_2 = 573 \pm 10$ nm. The asymmetric gap has at its narrowest position a width of ~ 28 nm. The length ratio is $\beta = 1.63 \pm 0.03$. The discontinuity visible in the center part of the mapping is ascribed to a polymer residue at the wire vicinity originating from the polymer matrix. The dimer in Figure 3b has a diameter of $D = 110 \pm 10$ nm and a gap width of ~ 16 nm. The length of the two wires are $L_1 = 830 \pm 10$ nm and $L_2 = 645 \pm 10$ nm, yielding a length ratio of $\beta = 1.29 \pm 0.03$. In both cases the average distance of the scan line to the nanowire surface is about 20 nm.

For the more asymmetric dimer in Figure 3a, the three first modes, marked by white dashed arrows and represented schematically on top of the mapping, reveal intense energy-loss maxima along only one of the wires and excitation of maxima at the position of the gap. In the case of the fourth and the fifth mode, we find two modes separated by a small energy difference of only 0.17 ± 0.02 eV that have the same number of maxima along the wires. For the lower-energy mode, the maximum at the position of the gap is missing, which indicates that a bonding-antibonding pair is created with only the antibonding mode being excited by the electron beam at this

position. If we compare for these two modes the intensity of the maxima in the middle of the short wire and the long wire, we find that here the maxima along the long wire are more intense for the bonding mode. The maxima of the antibonding mode are more intense along the short wire. For the long wire, this can only be judged on the basis of the maxima closer to the outer nanowire tip since for the position of the maxima closer to the gap a polymer residual leads to a discontinuity in the map. The difference in intensity of bonding and antibonding mode along the two wires is attributed to the ratio β being further apart from 1.5. Simulation of the multipole modes of the two nanowires with same dimensions as those in Figure 3a show that the energy of the $l = 3$-mode of the long wire is red-shifted by 0.05 ± 0.02 eV from the $l = 2$-mode of the short wire. We find that this energy difference results in mode hybridisation displaying different intensities for the two wires. The simulation in Figure 3a shows us mode coupling between the $l = 3$ and $l = 2$ modes of the two wires. The two images show the corresponding field distributions for bonding and antibonding modes. This result is consistent with previously published calculations.[16] However in their case, only the coupling of the dipolar modes was investigated.

For the dimer in Figure 3b the length ratio is $\beta = 1.29 \pm 0.03$. This value is in the range of the symmetry-broken dimers discussed in Ref. 16 where coupling of the two dipole modes of the two wires was investigated. In our case, we do not find evidence for mode coupling between the dipole modes here. The discrepancy is possibly due to the higher aspect ratio of the wires in Figure 3b that leads to narrower resonances and thus limiting the spectral overlap between the dipolar modes of the two wires. Instead, we find broad maxima at the same energy along both wires (labelled with the white dashed lines number six and seven) that most probably results from mode coupling of the fourth-order mode of the long wire and the third-order mode of the short wire. At the position of the gap, the peak is much narrower which we attribute to the fact that at the position of the gap only the antibonding mode is excited. The value β of this dimer ($\beta = 1.29 \pm 0.03$) is close to $\frac{l_4}{l_3} = 1.33$. For a dimer with these dimensions, our simulation confirms the coupling between the $l = 4$-mode of the long wire and $l = 3$-mode of the short wire (see inset in Figure 3b). We find that for the nanowire dimers the effective wavelength scaling can provide indications to which of the modes are coupling. However, important parameters such as the gap size and the nanowire dimensions that influence the mode coupling are not taken into account.

3 Experimental

AuAg nanowire dimers were synthesized by electrochemical deposition of segmented nanowires in ion-track etched polymer templates.[25,40,41] The first process step consists of the irradiation of 30 μm thick polycarbonate templates with Au ions of energy 2 GeV at the UNILAC linear accelerator at the GSI Helmholtz Center. When passing through the foil, each individual ion projectile produces a straight nano-sized damage trail. The ion tracks in the irradiated polymer are chemically dissolved and transformed into nanochannels.[42] A thin Au layer is sputter coated on one side of the foil serving as a cathode for the subsequent electrochemical deposition process. The Au layer is reinforced electrochemically by a Cu layer, grown in a two electrode arrangement at -0.5 V vs Cu anode. Segmented nanowires are created in the nanochannels by pulsed deposition in a three-electrode arrangement from a single-bath electrolyte. A Pt coil is used as the anode and a Ag/AgCl (sat. KCl) electrode as reference. The electrolyte consists of 50 mM $KAu(CN)_2$, 20 mM $KAg(CN)_2$, and 0.25 M Na_2CO_3 in aqueous solution. A pulse sequence consisting of -1.1V/-0.5V/-1.1V vs reference electrode is chosen to deposit nanowires consisting of three segments with concentrations $Au_{60}Ag_{40}$/ $Au_{15}Ag_{85}$/ $Au_{60}Ag_{40}$, respectively. After dissolution of the polymer template and suspension of the nanowires in isopropanol, few drops of the suspension are pipetted on a 30 nm thick Si_3N_4 film (Plano). After evaporation of the isopropanol, the segmented nanowires are randomly distributed on the substrate. The substrate with the wires is dipped for 3 h in nitric acid and finally cleaned in series with deionized water and dichloromethane. The nitric acid dissolves the Ag in the Ag-rich segments selectively. For the Au-rich segments the AuAg overall composition is not changed. This can be explained since due to the high Au content, the surface is quickly passivated by Au atoms. Only Ag atoms on the wire surface are dissolved, leading to a thin Au shell on the nanowire surface. The method thus leads to the formation of two Au-rich wires separated by small gaps.[24] While the majority of the resulting dimers consist of wires of similar lengths also dimers with large asymmetry are found. The nanowire dimer in Figure 2 was annealed at 300 °C for 30 min. This leads to a rounding of the nanowire tips and allows thus to improve the comparability between simulation and experimental data.

We focused our attention to asymmetrical dimers and investigated them by STEM-EELS in the Zeiss SESAM TEM, operated at 200 kV, at the Max Planck Institute for Intelligent Systems.[43] EELS linescans were acquired using a probe size of about 5 nm. Typically 100 spectra were acquired along the wire. Typical acquisition times were 1 s per spectrum. In order not to saturate the CCD camera, the energy-loss spectrum was spread perpendicular to the energy-dispersive direction. The energy spread of the electron beam was below 100 meV. The energy dispersion was set to 0.01 eV/channel using the MANDOLINE energy filter. The spectrometer acceptance angle was slightly larger than the convergence angle (3 mrad). After acquisition the energy was calibrated by setting all zero-loss peaks to 0 eV. For EFTEM, the energy spread

of the source was set to 0.23 eV. An energy-selecting slit of 0.2 eV was selected and energy-filtered images were acquired in the energy-loss range from -1 to +4 eV. This allowed calibrating the energy using the zero-loss peak. Acquisition times were automatically set for each image with a maximum of 30 s. The acceptance angle was limited by the objective aperture (typically 3 mrad). The convergence angle was well below 1 mrad. For both, EELS and EFTEM acquisition the background of the zero-loss peak was removed by fitting a power-law function to the high-energy tail of the peak.

We additionally simulated the surface plasmon resonances of different nanowires and nanowire dimers using the CST Microwave Studio finite element integration program and compared them to our experimental results. All nanowires in our simulations have hemispherical end caps. The surface plasmon modes are excited by a small dipole located one nanometre from one end of the structures. The dipole is oriented in the direction of the longitudinal axis of the nanowires. Data for the dielectric function of Au is taken from references 44 and 45.

4 Conclusions

In conclusion, EELS measurements on asymmetrical AuAg nanowire dimers synthesized by electrodeposition in ion-track etched polymer reveal up to nine different multipole modes spectrally clearly separated from each other. We demonstrate that by tuning the asymmetry of the dimer dimensions new modes can be generated. They result from the surface plasmon coupling between modes of differing multipole order of the two nanowires. Here, the coupling of high-multipole order modes of differing order in asymmetrical nanowire dimers is demonstrated for the first time. The comparison of the experimental data on AuAg dimers with finite element simulations on pure Au dimers reveals that in both cases the same resonances can be identified. The excellent agreement between our experimental results and the finite element simulation enables the design of more complex structures for sensing applications. For detailed knowledge on the position and intensity of the surface charge maxima for these complex structures, the STEM-EELS experiment is necessary.

References

1 N. J. Halas, S. Lal, W. S. Chang, S. Link and P. Nordlander, *Chem. Rev.*, 2011, **111**, 3913.

2 F. Hao, Y. Sonnefraud, P. Van Dorpe, S. A. Maier, N. J. Halas and P. Nordlander, *Nano Lett.*, 2008, **8**, 3983.

3 F. Hao, P. Nordlander, Y. Sonnefraud, P. Van Dorpe and S. A. Maier, *ACS Nano*, 2009, **3**, 643.

4 J. B. Lassiter, H. Sobhani, M. W. Knight, W. S. Mielczarek, P. Nordlander and N. J. Halas, *Nano Lett.*, 2011, **12**, 1058.

5 A. Artar, A. A. Yanik and H. Altug, *Nano Lett.*, 2011, **11**, 3694.

6 A. Christ, O. J. F. Martin, Y. Ekinci, N. A. Gippius and S. G. Tikhodeev, *Nano Lett.*, 2008, **8**, 2171.

7 D. J. Wu, S. M. Jiang and X. J. Liu, *J. Phys. Chem. C*, 2012, **116**, 13745.

8 J. Petschulat, D. Cialla, N. Janunts, C. Rockstuhl, U. Hübner, R. Möller, H. Schneidewind, R. Mattheis, J. Popp, A. Tünnermann, et al., *Opt. Express*, 2010, **18**. 4184.

9 G. Lu, J. Liu, T. Zhang, H. Shen, P. Perriat, M. Martini, O. Tillement, Y. Gu, Y. He, Y. Wang and Q. Gong, *Nanoscale*, 2013, **5**, 6545.

10 C. Wu, A. B. Khanikaev, R. Adato, N. Arju, A. A. Yanik, H. Altug and G. Shvets, *Nat. Mater.*, 2011, **11**, 69.

11 B. Lahiri, A. Z. Khokhar, R. M. De La Rue, S. G. McMeekin and N. P. Johnson, *Opt. Express*, 2009, **17**, 1107.

12 G. Bachelier, I. Russier-Antoine, E. Benichou, C. Jonin, N. Del Fatti, F. Vallée and P.-F. Brevet, *Phys. Rev. Lett.*, 2008, **101**, 197401.

13 S. Sheikholeslami, Y.-W. Jun, P. K. Jain and A. P. Alivisator, *Nano Lett.*, 2010, **10**, 2655.

14 N. W. Bigelow, A. Vaschillo, J. P. Camden and D. J. Masiello, *ACS Nano*, 2013, **7**, 4511.

15 C. Huang, X. Yin, L. Kong and Y. Zhu, *J. Phys. Chem. C*, 2010, **114**, 21123.

16 L. S. Slaughter, Y. Wu, B. A. Willingham, P. Nordlander and S. Link, *ACS Nano*, 2010, **4**, 4657.

17 A. L. Koh, K. Bao, I. Khan, W. E. Smith, G. Kothleitner, P. Nordlander, S. A. Maier and D. W. McComb, *ACS Nano*, 2009, **3**, 3015.

18 L. Shao, K. C. Woo, C. Fang, H. Chen, Z. Jin, J. Wang and H.-Q. Lin, *ACS Nano*, 2010, **4**, 3053.

19 L. Shao, C. Fang, H. Chen, Y. C. Man, J. Wang, J. and H.-Q. Lin, *Nano Lett.*, 2012, **12**, 1424.

20 F. Neubrech, D. Weber, J. Katzmann, C. Huck, A. Toma, E. Di Fabrizio, A. Pucci and T. Härtling, *ACS Nano*, 2012, **6**, 7326.

21 F. Neubrech, A. Garcia-Etxarri, D. Weber, J. Bochterle, H. Shen, M. Lamy de La Chapelle, G. W. Brayant, J. Aizpurua and A. Pucci, *Appl. Phys. Lett.*, 2010, **96**, 213111.

22 J. R. Krenn, G. Schider, W. Rechberger, B. Lamprecht, A. Leitner and F. R. Aussenegg, *Appl. Phys. Lett.*, 2000, **77**, 3379.

23 J. Aizpura, G. W. Bryant, L. J. Richter and F. J. Garcia de Abajo, *Phys. Rev. B*, 2005, **71**, 235420.

24 L. Qin, S. Park, L. Huang and C. A. Mirkin, *Science*, 2005, **309**, 113.

25 I. Alber, W. Sigle, S. Müller, R. Neumann, O. Picht, M. Rauber, P. A. van Aken and M. E. Toimil-Molares, *ACS Nano*, 2011, **5**, 9845.

26 I. Alber, W. Sigle, F. Demming-Janssen, R. Neumann, C. Trautmann, P. A. van Aken and M. E. Toimil-Molares, *ACS Nano*, 2012, **6**, 9711.

27 B. Willingham, D. W. Brandl and P. Nordlander, *Appl. Phys. B*, 2008, **93**, 209.

28 M. Abb, Y. Wang, P. Albella, C. H. de Groot, J. Aizpurua, O. L. Muskens, *ACS Nano*, 2012, **6**, 6462.

29 Computer Simulation Technology, www.cst.de.

30 L. Burr, I. Schubert, W. Sigle, C. Trautmann and M. E. Toimil-Molares, unpublished work

31 J. Nelayah, M. Kociak, O. Stéphan, F. J. García de Abajo, M. Tencé, L. Henrard, D. Taverna, I. Pastoriza-Santos, L. M. Liz-Marzán and C. Colliex, *Nat. Phys.*, 2007, **3**, 348.

32 M. W. Chu, V. Myroshnychenko, C. H. Chen, J. P. Deng, C. Y. Mou and F. J. García de Abajo, *Nano Lett.*, 2009, **9**, 399.

33 B. Schaffer, W. Grogger, G. Kothleitner and F. Hofer, *Ultramicroscopy*, 2010, **110**, 1087.

34 D. Rossouw, M. Couillard, J. Vickery, E. Kumacheva and G. A. Botton, *Nano Lett.*, 2011, **11**, 1499.

35 F. J. García de Abajo, *Phys. Rev. B*, 1999, **59**, 3095.

36 F. J. García de Abajo, *Phys. Rev. Lett.*, 1999, **82**, 2776.

37 F. J. García de Abajo and M. Kociak, *Phys. Rev. Lett.* 2008, **100**, 106804.

38 B. Schaffer, G. Kothleithner, W. Grogger, *Ultramicroscopy* 2006, **106**,

1129-1138.
39 L. Novotny, *Phys. Rev. Lett.*, 2007, **98**, 266802.
40 M. E. Toimil-Molares, *Beilstein J. Nanotechnol.*, 2012, **3**, 860.
41 C. Trautmann, In *Ion Beams in Nanoscience and Technology*, ed. R. Hellborg, H. J. Whitlow and Y. Zhang, Springer: Berlin Heidelberg, 2010; pp. 369-387.
42 C. Trautmann, *Nucl. Instrum. Methods Phys. Res. B*, 1995, **105**, 81.
43 C. T. Koch, W. Sigle, R. Höschen, M. Rühle, E. Essers, G. Benner and M. Matijevic, *Microsc. Microanal.*, 2006, **12**, 506.
44 M. A. Ordal, R. J. Bell, R. W. Alexander Jr, L. L. Long and M. R. Querry, *Appl. Optics*, 1985, **24**, 4493.
45 P. B. Johnson and R. W. Christy, *Phys. Rev. B* , 1972, **6**, 4370.

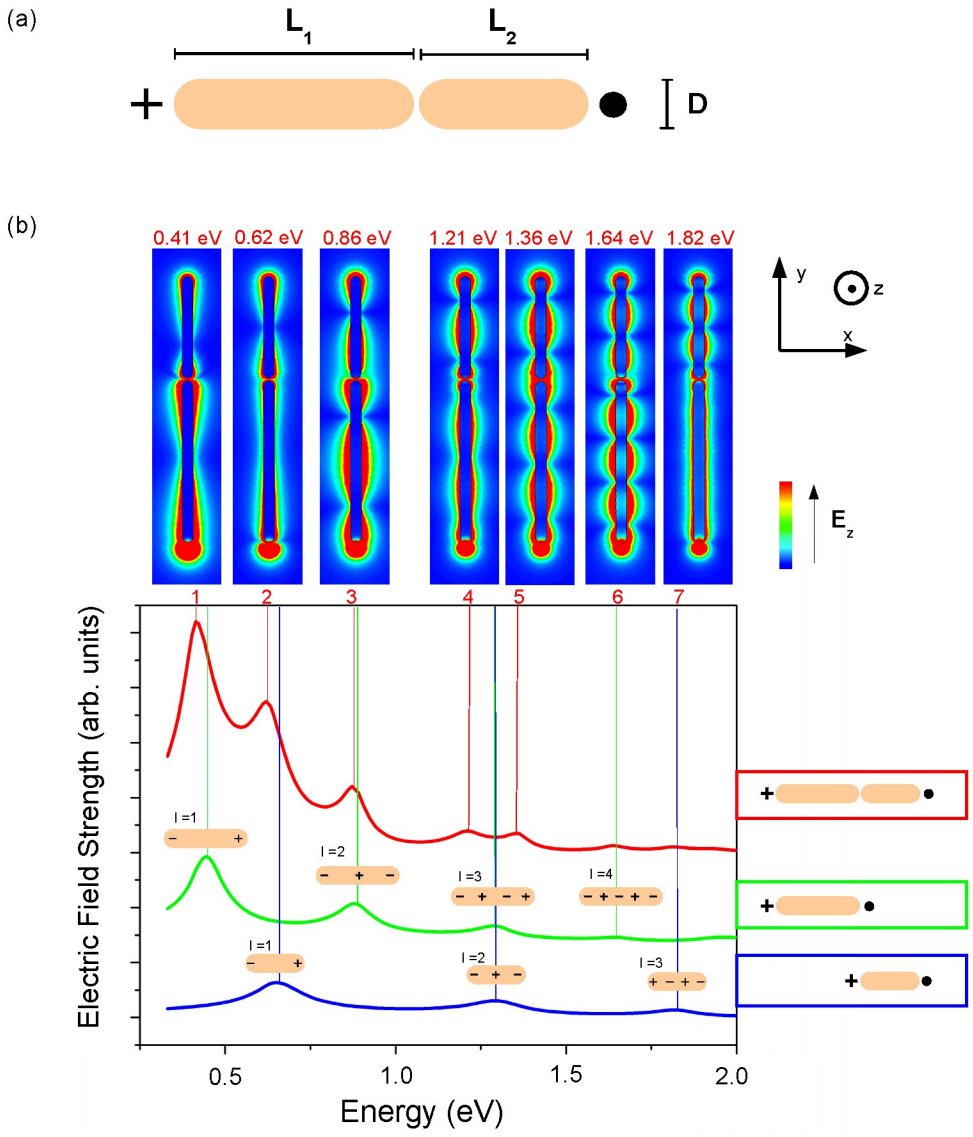

Fig. 1 (a) Schematic image of a nanowire dimer with dimensions L_1, L_2 and D. The position of the dipole exciting the plasmons (black cross) and where the electric field was calculated (black dot) are marked in the schemes. (b) Electric field strength vs excitation energy for surface plasmons in a long single nanowire ($L_1 = 1036$ nm, green spectrum), a short single wire ($L_2 = 656$ nm, blue spectrum) and an asymmetrical dimer (red) consisting of the two wires of same dimensions L_1 and L_2 separated by a small gap of 12 nm. The diameter of all structures is $D = 76$ nm. Schematics of the structures are shown on the right of the corresponding spectra. For the dimer modes, the E_z component of the excited field is shown on top of each of the peaks.

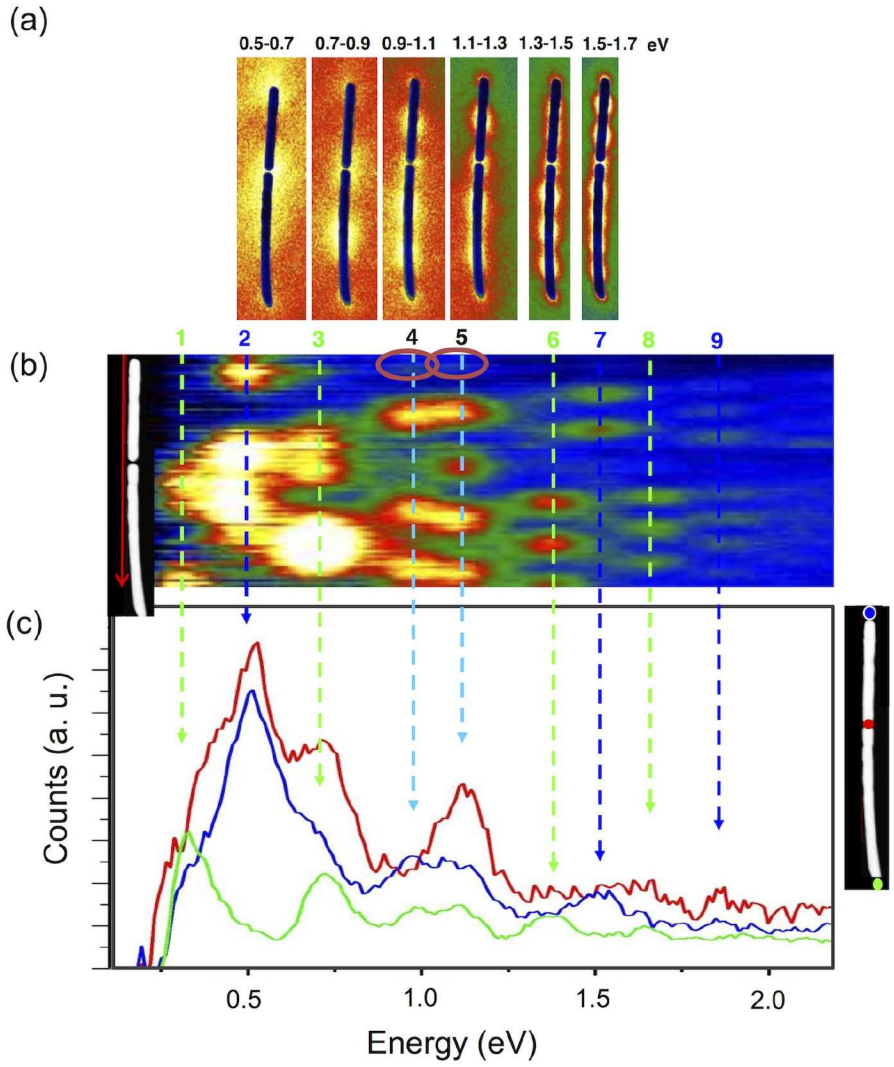

Fig. 2 (a) EFTEM series of a dimer with the same dimensions as in the simulation in Figure 1. (b) STEM-EELS map of the same dimer as in (a), consisting of 102 spectra measured along the length of the red arrow in the TEM image. The color indicates the energy-loss probability. Each horizontal line corresponds to one spectrum. (b) Three energy-loss spectra measured at the positions of the colored dots in the TEM image on the right. The color of the dots are the same as the color of the corresponding spectra.

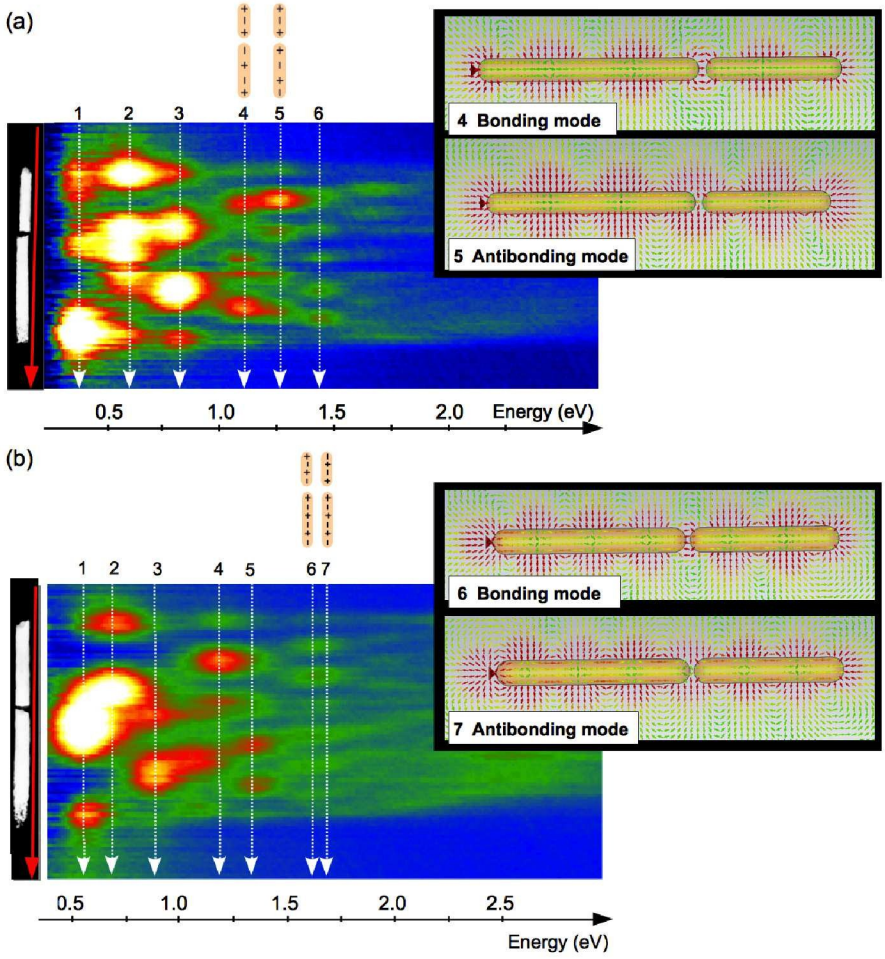

Fig. 3 (a) EELS scan consisting of 100 spectra along an asymmetrical dimer with $D = 100 \pm 10$ nm and $L_1 = 935 \pm 10$ nm and $L_2 = 573 \pm 10$ nm. The gap size is ~ 28 nm. (b) Scan consisting of 100 spectra along a dimer with $D = 110 \pm 10$ nm and $L_1 = 830 \pm 10$ nm and $L_2 = 645 \pm 10$ nm. The gap size is ~ 16 nm. The different modes are marked by white arrows and the field distributions are shown schematically on top of the modes. On the right of figure a and b the simulated field distributions for the bonding and antibonding mode of Au dimers with these dimensions are shown.